Article:
Burluka, A.A., Gaughan, R.G., Griffiths, J.F. et al. (3 more authors) (2016) Turbulent burning rates of gasoline components, Part 2 – Effect of carbon number. Fuel, 167. pp. 357-365. ISSN 0016-2361

https://doi.org/10.1016/j.fuel.2015.11.068

Turbulent Burning Rates of Gasoline Components, Part 2 - Effect of Carbon Number

A.A. Burluka[a], R.G. Gaughan[b], J.F. Griffiths[c], C. Mandilas[a,*], C.G.W. Sheppard[a], R. Woolley[d]

[a] School of Mechanical Engineering, The University of Leeds, Leeds LS2 9JT, UK

[b] ExxonMobil Research and Engineering Company, Paulsboro Technical Center, 600 Billingsport Road, Paulsboro, NJ 08066, United States

[c] School of Chemistry, University of Leeds, Leeds, LS2 9JT, United Kingdom

[d] The University of Sheffield, Department of Mechanical Engineering, Mappin Street, S1 3JD, UK

[*] Corresponding author. Present address: The Centre for Research and Technology, Hellas, Chemical Process & Energy Resources Institute, 3km Charilaou-Thermi Road, Thermi 57001, Greece

Abstract

Experimental measurements of turbulent and laminar burning velocities have been made of premixed hydrocarbon-air flames of straight chain molecules of increasing carbon number (from n-pentane to n-octane). Measurements were performed at 0.5 MPa, 360 K and turbulent velocities of 2 and 6 m/s for a range of equivalence ratios. The laminar burning velocities were used to interpret the turbulent data, but were also found to be broadly in line with those of previous workers. The equivalence ratio of the mixtures at which the maximum burning velocities occurred in the turbulent flames was richer than that under laminar conditions. The equivalence ratio of the peak turbulent burning velocity was found to be a function of the carbon number of the fuel and the turbulent intensity and became increasingly fuel rich with increases in each of these values.

1. Introduction

This is the second part of a two paper series presenting the measurement of turbulent burning velocities for hydrocarbons of different molecular structure under conditions typical of those seen in industrial applications. The main aim of the current work was to investigate the effects of fuel molecular structure and equivalence ratio, ϕ, on the laminar and turbulent burning velocity of deflagrations and allow for

direct comparison. The turbulent burning velocity is a function of those physico-chemical features of a fuel-air mixture encapsulated in its laminar burning velocity, u_l, and the turbulence characteristics of the flow field within the engine. The influence of fuel structure on the laminar burning velocity has been reported [e.g. 1-5]. However, experimental studies on the influence of hydrocarbon molecular structure on burn rate under turbulent conditions typical of those seen in industrial applications are sparse [6-7].

Presented in this paper are experimentally determined turbulent and laminar burn rates for a set of straight chain hydrocarbons of varied carbon number, n-pentane, n-hexane, n-heptane and n-octane. These fuels are representative components of automotive gasoline blends. Measurements of the laminar burning velocity of these fuels have been performed by a number of previous workers at a range of conditions [2, 4, 8-9]. Apart from the size of the carbon chain, which affects the number of breakdown steps needed during oxidation, another significant difference anticipated to have impact on burn rate, is the differing molar mass of the fuels selected for this study and, thus, their differing Lewis Number (or Markstein Number). This is expected to be especially important under turbulent conditions, as there is plenty of experimental evidence demonstrating the significance of fuel diffusion in premixed turbulent flames.

2. Experimental

Only brief details of the experiments are given here, further information can be found in Part 1 of this paper [10]. The Leeds MkII spherical bomb operating under laminar and turbulent conditions, was employed for the studies. The effects on burn rate of two different turbulent r.m.s. velocities were examined (u' = 2 m/s and 6 m/s). All experiments incorporated schlieren-based imaging. Laminar flames were recorded at 2000 frames/s. Turbulent flames were photographed at rates of 6300 and 9000 frames/s, for u' = 2 and 6 m/s, respectively. All deflagrations were initiated with a spark at a nominal initial temperature of T_i = 360 K and pressure of P_i = 0.5 MPa and were conducted for a range of equivalence ratios, from lean ($\phi \sim 0.8$) to rich ($\phi \sim 1.6$).

At least two laminar and five turbulent deflagrations were performed at each condition. For laminar flames, the repeatability tolerance was set at a maximum of 2% in the time elapsed from ignition required to reach a pressure of 0.75 MPa for tests conducted on the same day; and 3% for tests conducted on different days. Turbulent tests exhibited inherent cyclic variability and thus a similar

tolerance approach could not be followed; typical experimental scatter for turbulent flames was circa 10% (in coefficient of variance, COV), independent of the r.m.s. turbulent velocity.

3. Results and Discussion

3.1 Laminar flame propagation and cellular flames

As all the measurements in this study were performed at 0.5 MPa the majority of flames became 'cellular' shortly after ignition. The term 'cellularity' is used to describe the result of both hydrodynamic and thermo-diffusive instabilities observed in laminar flames where the flame surface develops irregular patterns, or 'cells', of varying dimensions. This phenomenon is known to accelerate the burn rate, by increasing the surface area of the flame and by modifying the composition of the flame front. Cellularity onset of expanding spherical flames has been predicted to occur when the flame reaches a certain critical radius, r_{crit}, and the ratio of thermal to mass diffusivity (i.e. the Lewis number, Le, of the deficient reactant [11-13]) exceeds unity. There may be other factors (such as heat loss, hydrodynamic stretch or gravity) which also affect the development of the cellular structure.

Identifying the onset of cellularity from experimental data can be ambiguous. For schlieren measurements, r_{crit}, has been defined as the point where small scale cells appear on the flame surface [11]. It is implicit, due to the progressively growing nature of these cracks, that definition of r_{crit} by photographic observations is subject to discrimination by the human eye and the quality of the optics employed. An alternative way of defining r_{crit} is by relating it to the point at which an appreciable flame acceleration (a_f) appears on the plot of stretched burning velocity (u_n) vs. mean flame radius [14, 15]. In the exemplar burn rate data of Figure 1, a noticeable a_f is typically observed at a radius of ca. 25 mm.

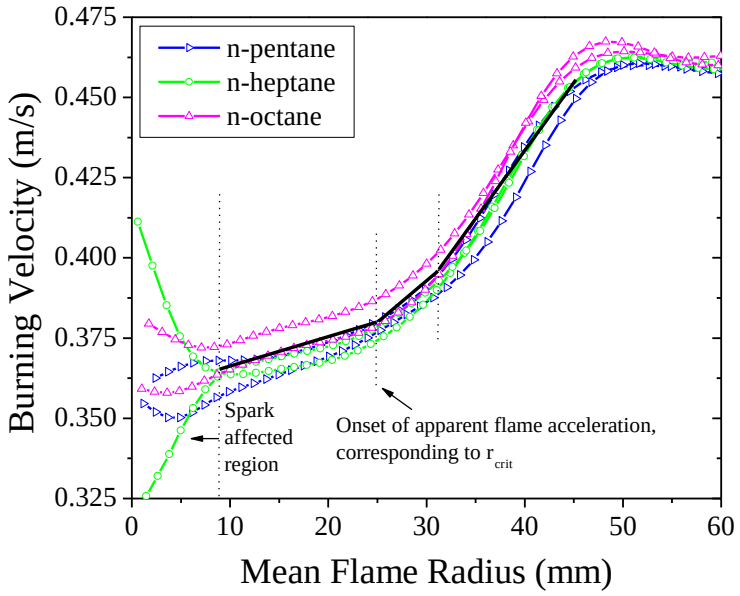

Figure 1 – Cellularity induced acceleration showing its graphically defined onset. Results displayed are for sample $\phi = 1.1$ flames.

For the vast majority of flames examined in the current study the difference between the visual determination of r_{crit} and that determined graphically [15] was within 1.5 ms (~3 frames), or 2-3 mm in mean flame radius. The values of r_{crit} displayed in Figure 2 are based on combined graphical and photographic evidence, the error is estimated at ±2 mm in radius.

For the alkanes investigated, r_{crit} decreased with ϕ and no major differences between the fuels were found at a given equivalence ratio. The latter observation correlates to some extent with values of burned gas Markstein length, L_b, plotted against r_{crit} (Figure 3).

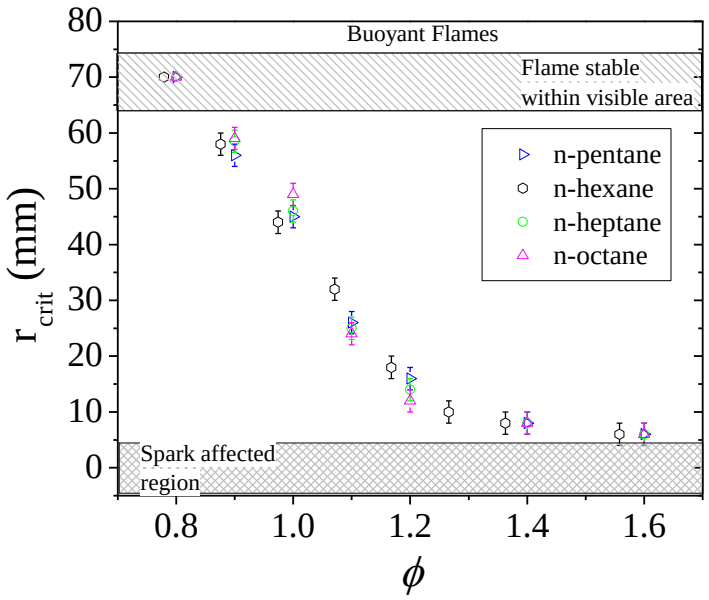

Figure 2 – Critical flame radii derived from photographic and graphical observations. Error bars of ± 2 mm are displayed.

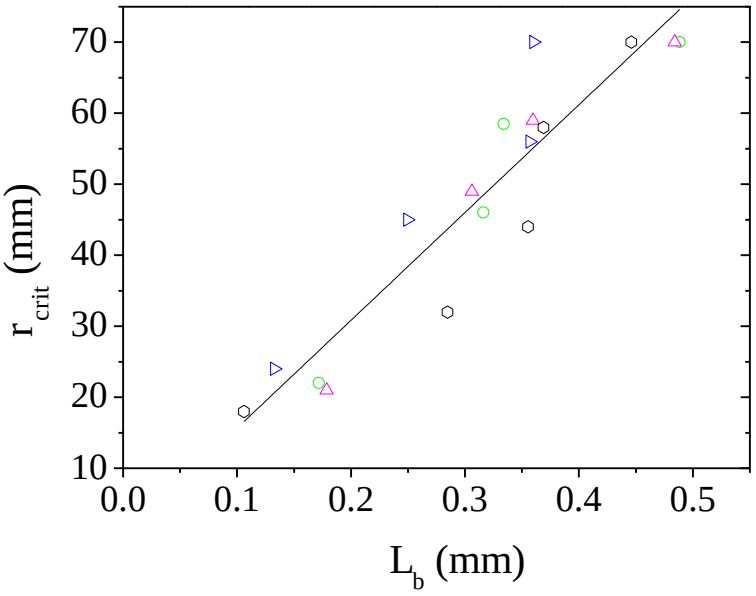

Figure 3 – Correlation between r_{crit} and L_b.

Of interest with respect to the effects of cellularity on flame propagation are the flame acceleration results, a_f, derived from stretched burning velocities, u_n, and shown in Figure 4. For the lean case (ϕ = 0.8) all flames remained smooth within the visible radius defined by the vessel's windows, as the

thermo-diffusive effects, coupled with stretch, stabilise the flame against the hydrodynamic instability. As a consequence, no acceleration due to cellularity was observed.

Typically for all fuels examined, for ϕ =1.1 following the spark affected region (i.e. for mean flame radius > 8 mm) flame acceleration was small and approximately constant up to around mean flame radii above 20 mm. At r_u > 20mm, acceleration increased, becoming significantly more marked at radii of 25 mm, which corresponds to r_{crit}. Thereafter, flames continued to accelerate quite sharply; reaching peak acceleration at 37-40 mm mean flame radii. Subsequently, flame acceleration fell, reaching low pre-cellularity rates by mean flame radii of circa 50 mm.

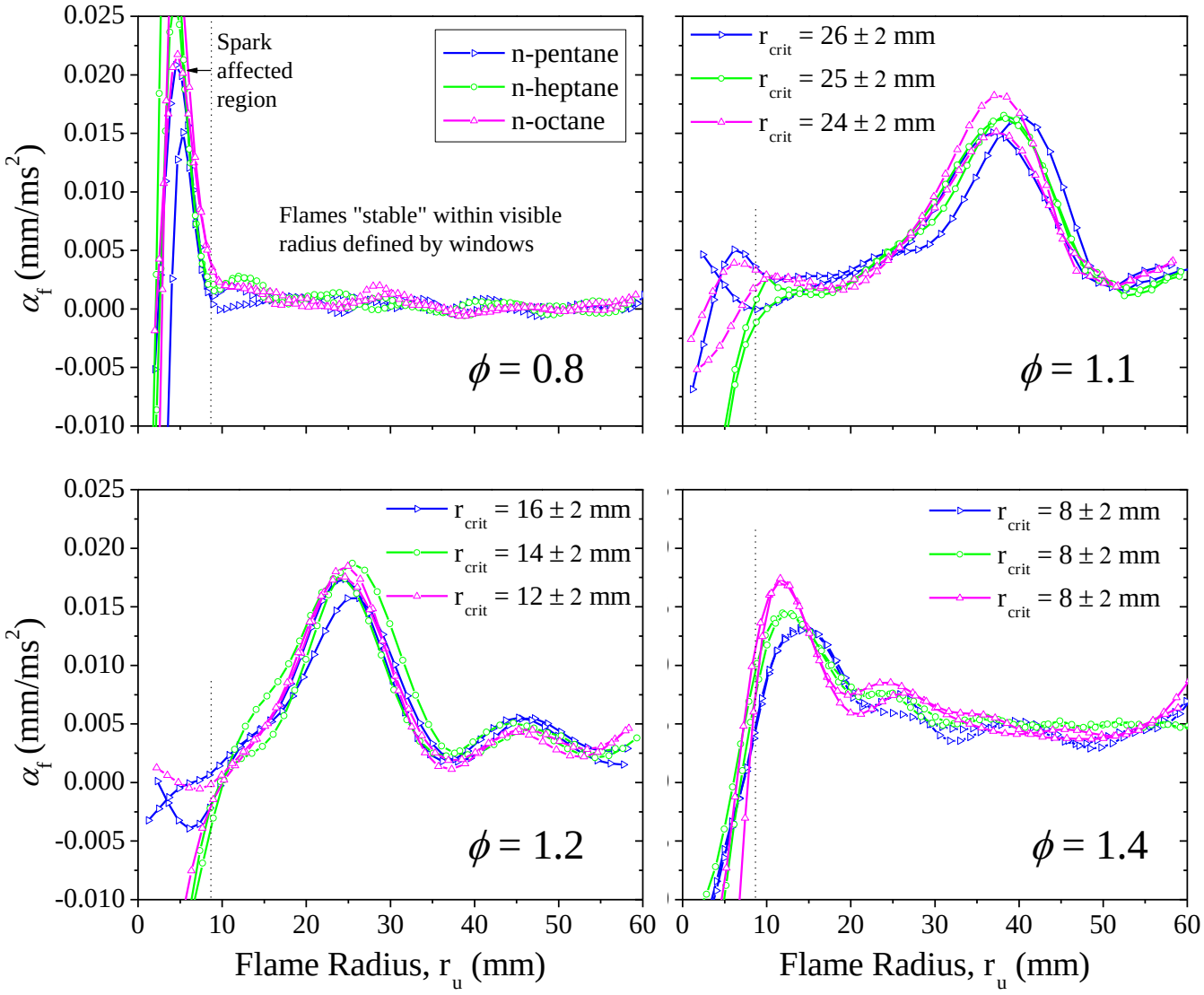

Figure 4 – Flame acceleration, $a_f = du_n / dt$, for different ϕ, highlighting the effects of cellularity on flame propagation.

The flames for ϕ =1.2 followed a similar pattern to ϕ =1.1, although with earlier development of cellularity (occurring soon after the spark affected region) the initial low and constant acceleration 'plateau' are less obvious, the peak accelerations and the return to low pre-cellularity levels occur sooner. A similar pattern can also be observed at ϕ =1.4, with even earlier cellularity development within the spark affected region.

The occurrence of significant flame acceleration at the critical flame radius for the onset of cellularity is caused by an associated increase in flame surface area [16]. An alternative, or possibly additional, reason for the increase in flame acceleration at the onset of cellularity arises from considerations of linear flame stability analysis based on high activation energy asymptotics [13]. The dynamics of a curved flame front dictate that, if the burning velocity is the same along the front, the trailing parts of a cell consume the fresh gas faster than the leading parts, per unit frontal area. A simple heuristic model predicted that flame acceleration will reduce to zero, when an equilibrium is attained between the leading and the trailing parts [17]. However, while the results shown in Figure 4 seem to support this model qualitatively, the theory assumes that flame perturbations (i.e. the depth of cells) are small compared to flame size, which is limited strictly to the initial acceleration period. In addition, numerical comparison is complicated by the effects of stretch rate, flame growth and short observation period.

To clarify the trend in a_f, cell size development was examined in schlieren images taken around the middle of the vessel window. To quantify the average cell size, the magnified grayscale flame images were further processed in MATLAB, first by converting them into black & white format and then by counting the number of pixels in each of the "white islands" corresponding to the flame cells, subsequently to obtain a mean cell flame area in mm^2. These average cell area results are displayed in Figure 5, for ϕ = 1.1 and 1.4. In general, average cell areas rapidly decreased after the onset of cellularity. For ϕ = 1.1, minimum cell areas generally occurred at flame radii of 10-15 mm after those at the onset of cellularity. For ϕ = 1.4, cells achieved their minimum size slightly faster (5-10 mm in mean flame radius after r_{rit}). Fully-developed cell areas for ϕ = 1.4 flames were 80% (for n-heptane and n-octane) smaller than those for the ϕ = 1.1 flames. With respect to the relative behaviour between the different fuels, the more diffusive (lower Le) n-pentane had the largest average, fully-developed cell area; followed by n-hexane and then n-heptane and n-octane. These results suggest a correlation between cell-size and flame acceleration. The point at which cell sizes attained their minimum values coincided well with that in reaching peak acceleration (plots of Figure 5 vs. Figure 4). Similar

correlations also existed between average cell areas and peak accelerations. This is consistent with flame acceleration resulting from the transition from a smooth surfaced flame into a fully cellular flame and its associated increase in flame surface area. Once a constant fully developed cell size is reached, the increase in flame surface area per unit volume of the flame ceases and flame acceleration returns the pre-cellular values.

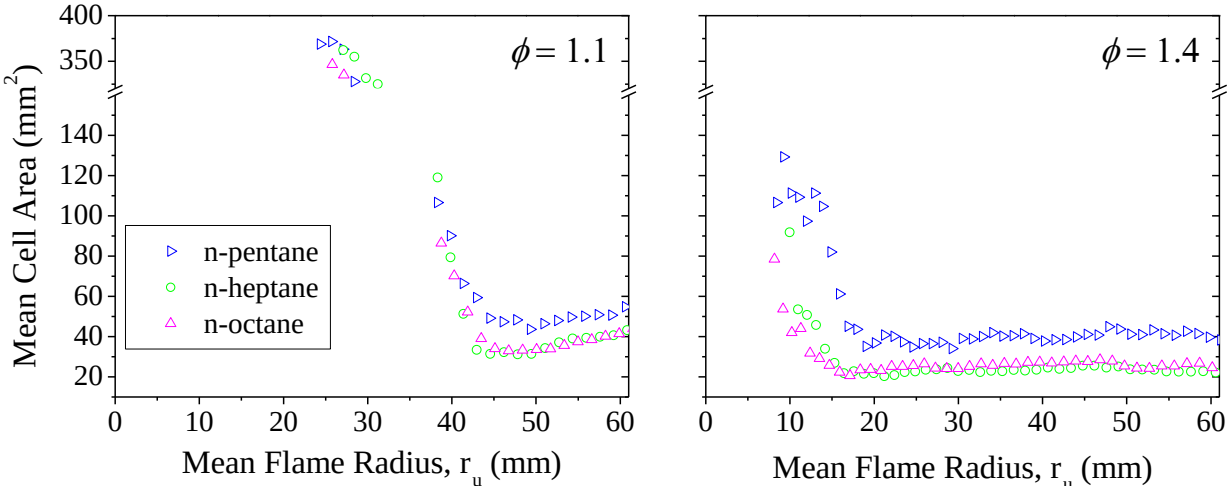

Figure 5 – Mean cell areas as determined from schlieren images of cellular flames.

3.1 Laminar Burning Velocity

Laminar burning velocity measurements, plotted against ϕ, are shown in Figure 6. Solid lines correspond to unstretched burning velocity data determined via the techniques described in [10]. Dotted lines correspond to u_l values computed using $u_l = u_{n,min}$ (i.e. $L_b = 0$), where, u_n is the stretched entrainment burning velocity. All rich flames for the alkanes examined showed signs of cellularity as early as a mean flame radius of 10-15 mm. Consequently, too few data points were available to determine L_b. Burning velocities obtained in this way cannot be considered to be rigorously defined but represent a pragmatic approach to obtaining laminar burning velocity data to aid the analysis of subsequent turbulent burning measurements.

All fuels studied were found to have their maximum u_l at $\phi \sim 1.1$. There was hardly any variation in u_l between lean fuel-air flames, as is also evident in the flame speed measurements by Davis and Law [2]

for 1 bar and 300 K. Increased laminar burn rates were apparent at fuel rich conditions for the sequence n-pentane to n-octane, although, as mentioned above, these data are not strictly defined u_l.

The Markstein length of a flame is a physico-chemical flame parameter, customarily used to characterise the effect of stretch rate on flame speed [14]. High positive values of L_b indicate that as the flame expands, and becomes increasingly less stretched, there is a gain in flame speed; the opposite is true for flames with negative Markstein length values. For reasons already explained, Markstein lengths could not be determined for $\phi > 1.1$, hence results displayed here refer to fuel-air mixtures of up to $\phi = 1.1$ (Figure 7). Positive values of L_b were measured for all fuels. Differences between the fuels were within experimental scatter, nonetheless, the lightest n-pentane was measured to have consistently lower Markstein lengths, while the heaviest n-octane had consistently the higher L_b.

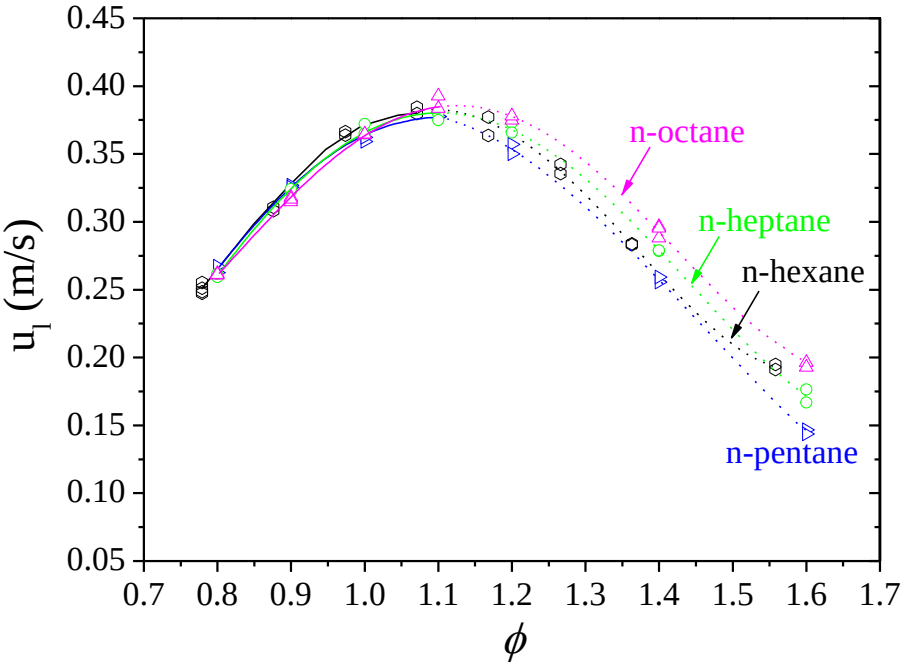

Figure 6 – Stretch-free laminar burning velocities for n-alkanes, plotted against ϕ. Dotted lines correspond to u_l values computed using $u_l = u_{n,min}$.

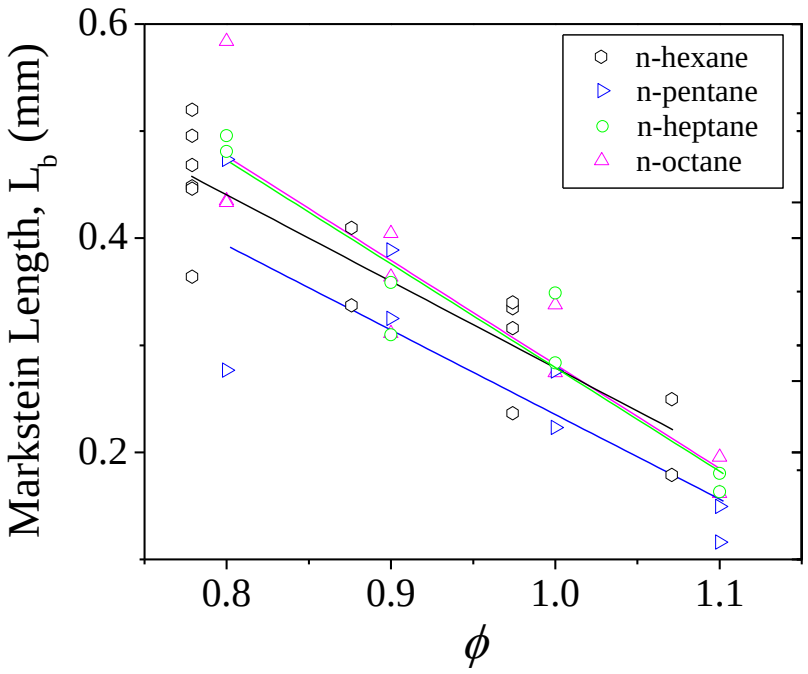

Figure 7 – Measured burnt Markstein lengths of the n-alkanes, plotted against ϕ. Values of L_b of $\phi > 1.1$ mixtures could not be determined as flames became cellular too early following spark discharge.

The experimentally determined values of u_l were compared with Chemkin Premix code [18-19] at the same unburned temperature and pressure. Multi-component formulation for transport properties including Soret diffusion were used. The JetSurF 2.0 mechanism [20] was selected as it has been previously compared with laminar burning measurements [5] at elevated conditions and it was possible to compare eight of the fuels considered with a single mechanism. The comparison is shown in Figure 8. There is good agreement between the experiments and model at lean ϕ. For $\phi > 1.1$, the flames were cellular shortly following ignition so the experimental data corresponds to the minimum burning velocity recorded. It is to be expected that cellularity increases the burn rate, so it might be presumed that the measured values are higher than the computed values. The comparison is to some extent meaningless as the flames do not exist as a single uninterrupted flame front under these conditions as thermo diffusive effects would result in localized quenching of the flame surface [14]. However, the computed u_l could provide a useful, unambiguously defined reference although they cannot be experimentally verified.

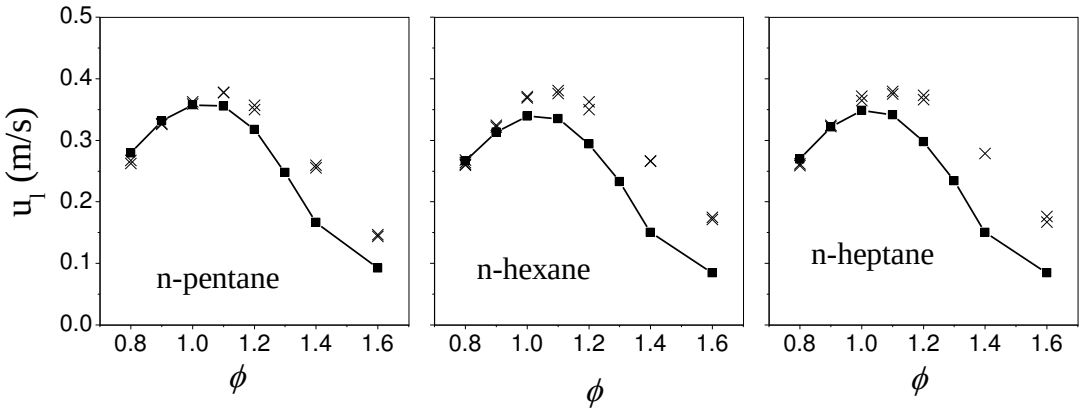

Figure 8 – Comparison of experimental burning velocity (crosses) with numerical computations (filled squares) performed with Jetsurf 2.0. Initial temperature and pressure 360 K and 0.5 MPa.

The development of hydrocarbon kinetic mechanisms, allied with improvements in u_l experimental methods, has resulted in better understanding of the key combustion processes taking place within the flame [4-5, 21-24]. Unimolecular decomposition of the primary fuel can readily occur at the temperatures that prevail in the reaction zone of a premixed flame, promoted by kinetic energy transfer during collisions between molecules. The weakest bonds within the primary fuel, the saturated C-C linkages, are the most susceptible to fragmentation. However, there is another possibility for decomposition of the longer chain n-alkanes (e.g. at C > 5) due to the flexibility of the molecular chain. In this process intramolecular energy transfer may occur as a result of one end of the chain colliding with a site at or close to the other end [25]. This is illustrated in Figure 9 as an interaction between a primary and a secondary bound H atom, and the inference is that excess energy would accumulate in one or other of the C-H bonds. The secondary C-H bond would be the more susceptible of the two to decomposition, by virtue of its lower bond strength, but the main significance is that fragmentation must yield an alkyl radical and an H atom, rather than the, predominantly, two alkyl radicals in the more general intermolecular collisional process. As in unimolecular reactions, the rate at which the decomposition can occur is limited by the vibrational frequency of the bond to be broken and a statistical (or steric) factor which relates to the probability of the intramolecular interaction taking place. This route for H atom generation can only contribute to the burn rates measured for the longer chain n-alkanes (n-hexane, n-heptane and n-octane) under fuel rich conditions.

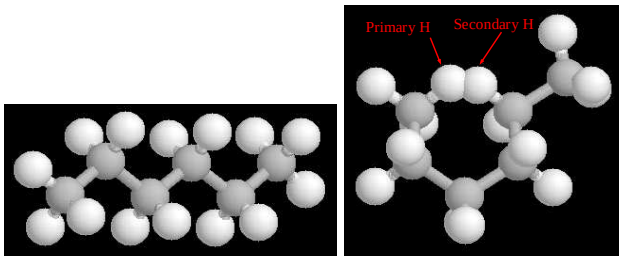

Figure 9 – Normal hexane molecule (left) and conformation leading to intra-molecular collision between H atoms (right).

3.2 Turbulent Burning Velocity

Displayed in Figures 10 and 11 are burn rates for the n-alkane dataset, under turbulent r.m.s. velocities of u' = 2 and 6 m/s, plotted versus ϕ. The curves are 3rd order polynomial fits to the experimental data. The experimental scatter in u_{te} was ~10% COV and proved independent of *u'*. This was in accord with previous measurements in this vessel [26].

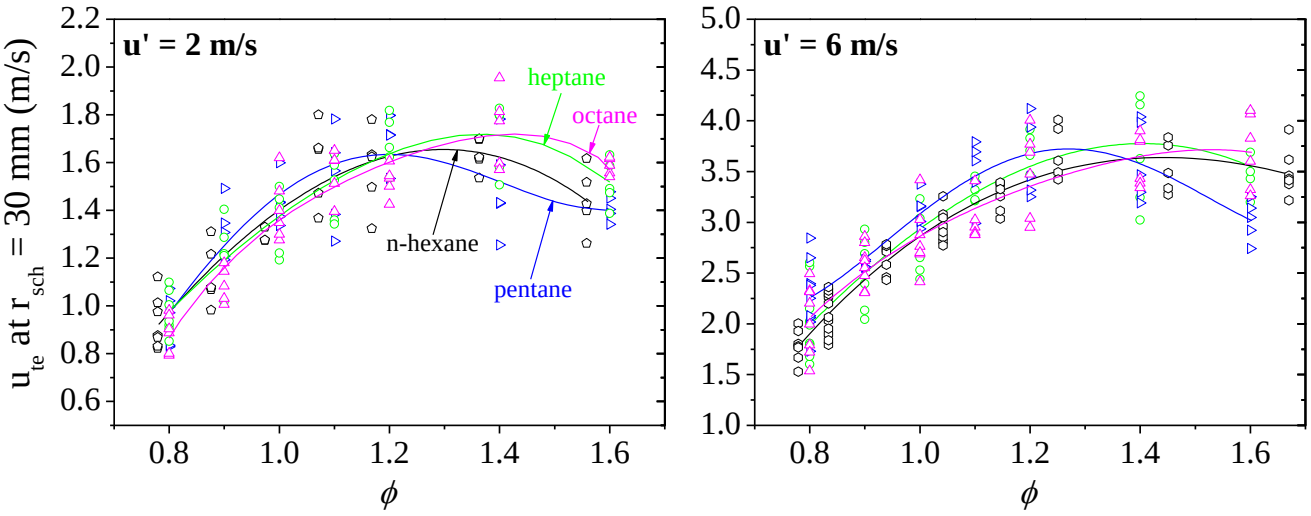

Figure 10 – Entrainment turbulent burning rates of alkanes at r_{sch} = 30 mm, plotted against ϕ.

The maximum turbulent burning velocities were attained in rich mixtures and the ϕ at which they were observed increased with fuel molecule size. Also as *u'* increased peak u_{te} values shifted further towards rich mixtures. This is a qualitative difference between turbulent and laminar flames, as the laminar

flames generally burn fastest at $\phi \sim 1.1$. The degree of enhancement, expressed as u_{te} / u_l, is shown in Figure 12 and can be seen to vary both with the fuel and ϕ.

The peak u_{te} values obtained were similar for all alkane fuels tested. For $u' = 2$ m/s the maximum u_{te} was ~ 1.7 m/s and at $u' = 6$ m/s it was ~ 3.7 m/s (values obtained from the maxima of the third order fits). In comparison, peak laminar burn rates were 0.35 to 0.38 m/s. Overall, the increase in the maximum u_{te} attained by increasing u' from 2 to 6 m/s accorded to $u_{te,max} \sim (u')^{0.73}$, which is similar to that described by Zimont [27]. For fuel lean conditions the values of u_{te} are similar for n-pentane to n-octane. Apparent differences between the flames were observed at fuel rich conditions. It could thus be argued that fuel effects were not observed to be significant for conditions where fuel was the deficient reactant.

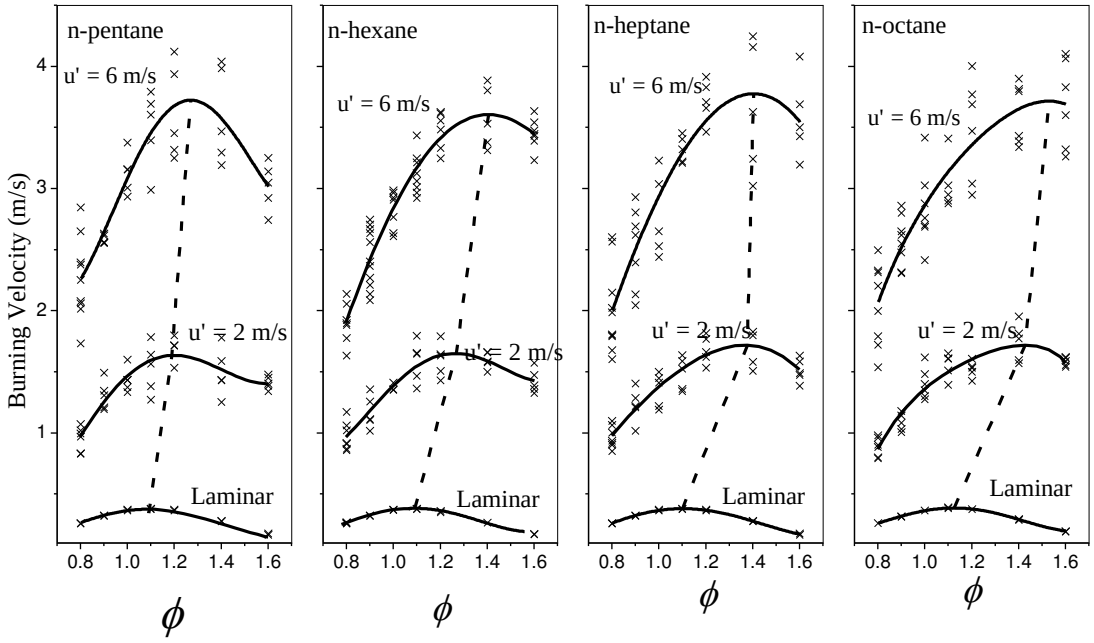

Figure 11 – Laminar and turbulent burning velocities for the normal alkanes. The dashed lines connect the maximum at each condition.

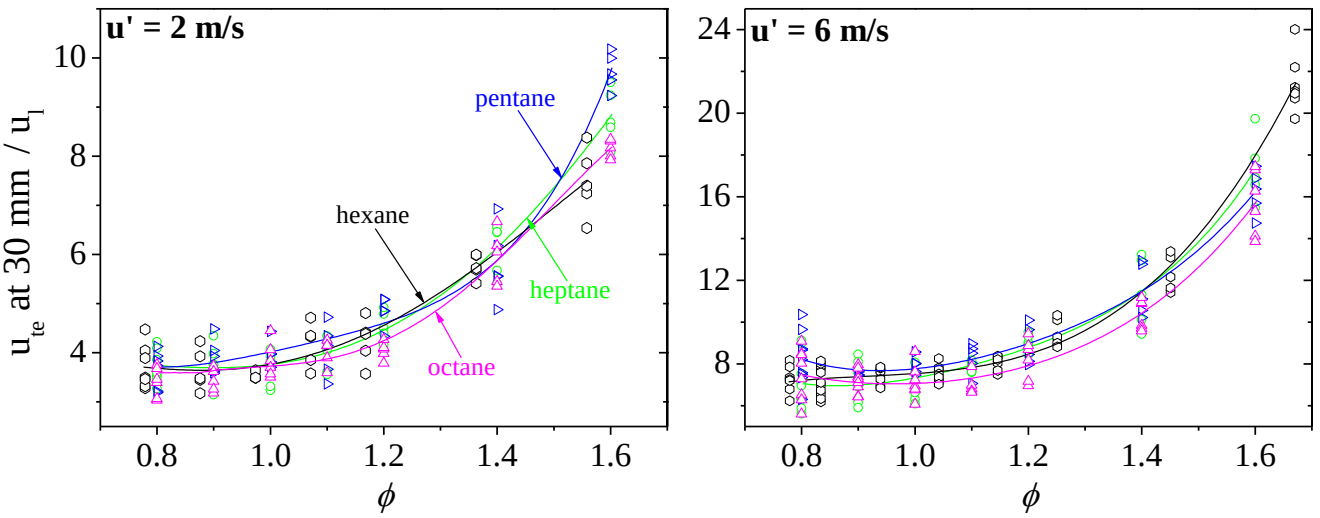

Figure 12 – Ratio of turbulent over laminar burning velocities plotted against ϕ, quantifying the burn rate gains due to turbulence for the various n-alkanes investigated.

Displacement of the maximum burning rate towards rich mixtures was observed as early as 1955 [28]; however, this observation received little attention until relatively recently [29]. There have been numerous studies comparing turbulent flames with the same laminar burning velocity but differing thermo-diffusive properties, some of which are summarized in [29]. These have repeatedly demonstrated that flames with lower Lewis numbers (or Markstein numbers) burn faster under turbulent conditions. Experimental measurements of turbulent flames with low Markstein numbers have identified changes in the structure in the flame front associated with the local curvature [30-31], as have DNS studies [32]. Where the flame front is convex to the unburned reactants, high radical concentrations are observed, with localized quenching occurring where the flame is concave. It seems likely that this phenomenon occurred in the rich hydrocarbon flames investigated here. “Finer-grained” wrinkling (compared to flames with high Markstein numbers) has also been associated with these flames [33].

A number of DNS studies examining the combustion of low Lewis number premixed flames have been performed [32, 34, 35]. Not only have these reproduced the experimental observations qualitatively [32] but also they have provided a detailed analysis of the burning process in lean hydrogen/air and hydrogen/methane/air flames. Lengths of intense burning bordered by areas of local flame extinction have also been identified. As a result, of the information that is available with DNS, it was possible to track the fuel decomposition as it flowed into both an intense burning ‘cell’ and an extinguished cusp [35]. Despite these revealing studies it is difficult to interpret the fuel sensitivity at rich ϕ of the flames

investigated here. In this case, the deficient reactant is molecular oxygen and so it would be expected that it is the diffusion of this molecule that creates region of intense burning and cusp formation. There is an excess of fuel and it seems unlikely that the diffusion of fuel should have any impact on the burn rate and hence any influence of the fuel on ϕ at which peak burning occurs seems unlikely. Under lean conditions where the fuel is the deficient reactant, little influence of the fuel was observed from n-pentane to n-octane.

Whilst there have been some attempts to incorporate these observations into turbulent burning velocity expressions and theories, notably by Bradley et al. [36], the laminar flame is often solely represented by u_l and so thermo-diffusive effects are neglected. If we consider the fuels and conditions that industrial flames are typically operated at, this is understandable. In order to correctly model thermo-diffusive effects in turbulent flames, alternative approaches are necessary. An older concept that is presently being reconsidered is that critically curved "leading points" of the flame front; i.e. those parts of the flame most advanced into the fresh gas lead the propagation. As these leading points are convex to the unburned mixture it has been suggested they are subject thermo-diffusive enhancement resulting in locally leaner (and faster) flames. Subsequently, Borghi et al. [37], made the alternative suggestion that the leading points are critically curved rather than strained. Recently, Venkateswaran et al. [38] have been able to correlate the turbulent consumption speed using the maximum stretched laminar burning velocity but could not collapse data for differing pressures. The leading edge hypotheses predicts that for heavier hydrocarbons the maximum turbulent burning rates should be exhibited by rich flames; however, the ϕ at which the maximum is attained should not depend on the turbulence level, which was observed here.

Despite recent advances in detailed computations there remains a demand for simpler expressions to predict the turbulent burning velocity, based on easily obtained parameters, although whether this is feasible is debatable. A study with iso-octane demonstrated that a selection of the existing expressions were unable to capture the trend of u_t with ϕ [39]. A number of workers have attempted approximate quantification of the influence of Markstein number on burn rate for turbulent premixed combustion [40-41]. Displayed in Figure 13 are average experimental u_{te} / u_l values, generated in the current study, plotted against L_b. A consistent trend was observed, with the ratio of u_{te} / u_l decreasing with L_b for each of the two r.m.s. turbulent velocities; similar effects were described in [26, 33]. Results such as this may well form the basis of future empirical turbulent burning velocity expressions.

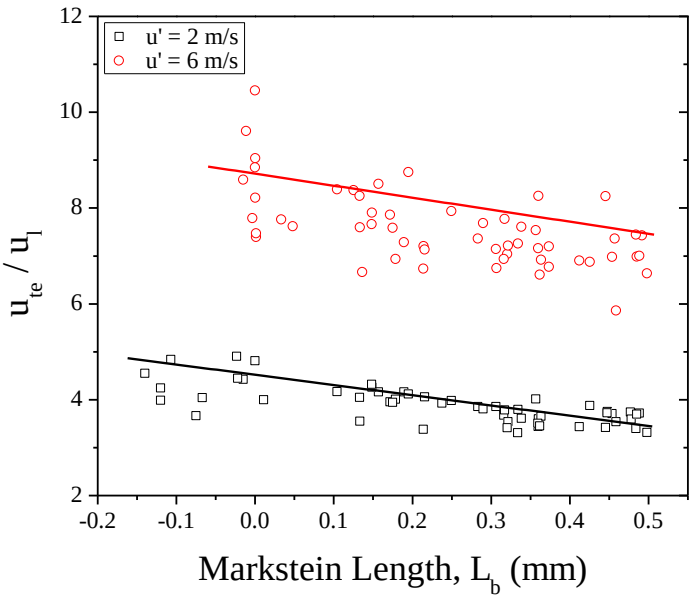

Figure 13 – Overall correlation of u_{te} / u_l with L_b of alkanes of C_3-C_8 and C_6 hydrocarbons for equivalence ratios of $0.8 \leq \phi \leq 1.2$, for turbulent r.m.s. velocities of 2 m/s and 6m/s. Data from current work and [10, 15].

4. Conclusions

In his review of premixed turbulent combustion, Driscoll [42] asked the question ‘‘how important are thermodiffusive effects for fully turbulent conditions?’’. Using available experimental and numerical studies he found evidence that thermodiffusive effects are significant even in highly turbulent flames; this is confirmed with these experiments. In the majority of experimental studies examining this phenomenon flames of identical laminar burning velocity but differing Markstein (or Lewis) numbers have been compared. Whilst the above approach is useful at demonstrating this phenomenon this study demonstrates that fuel, equivalence ratio and turbulence levels are all of significance. The complexity of the combustion of premixed turbulent flames seems to increase as more wide ranging modelling studies and extensive experimental databases are presented. However, there remains the requirement for relatively simple expressions to predict the turbulent burning velocity within models of industrial applications and the results presented here may point towards future developments in this area.

- The laminar burning velocity of n-pentane, n-hexane, n-heptane and n-octane were found to almost identical for equivalence ratios varying from ca. 0.8 to 1.1. Under rich conditions u_l could not be measured as the spherically laminar flames were observed to be cellular from ignition. In

these cases u_l was estimated using the minimum observed flame speed, $u_{n,min}$. Values of $u_{n,min}$ increased with carbon number.

- Under laminar conditions at 0.5 MPa, cellularity enhances the burn rate. However, findings from the current study suggest that (for the rig used in this study, the fuels and conditions explored) cellularity-induced flame acceleration lasts for typically 15-20 mm following the cellularity onset, before returning back to values similar to those observed during the pre-cellular phase. Thermodynamic flame instabilities noted under laminar conditions did not appear to have any effects under corresponding turbulent conditions.
- The peak turbulent burning velocity did not occur at the same ϕ to the u_l. The peak turbulent burning velocity shifted to increasing ϕ under turbulent conditions. The magnitude of the shift increased with length of carbon chain and turbulence intensity. For instance, in the case of n-octane at u' = 6 m/s the peak turbulent burning velocity occurred at ϕ = 1.5 compared to the peak in u_l at ϕ = 1.1.
- At lean ϕ, the turbulent burning velocity was observed to be similar for the four fuels studied. The magnitude of peak turbulent burning velocity was also measured to be similar. However, at rich fuel conditions, there were notable differences between the turbulent burn rates of the alkanes examined.

Acknowledgements

The support of Mercedes-Benz High Performance Engines is gratefully acknowledged.

References

1. Gerstein, M., Levine, O., Wong, E.L., J Am Chem Soc 73 (1951) 418
2. Davis, S.G., Law, C.K., Combust Sci Technol 140 (1998) 427
3. Vagelopoulos, C.M., Egolfopoulos, F.N., P Combust Inst 27 (1998) 513
4. Farrell, J.T., Johnston, R.J., Androulakis, I.P., SAE Tech Paper (2004) 2004-01-2936
5. Wu, F., Kelley, A.P., Law, C.K., Combust Flame 159 (2012) 1417
6. A.A. Burluka, R.G. Gaughan, J.F. Griffiths, C. Mandilas, C.G.W. Sheppard, R. Woolley, 7th European Combustion Meeting, Budapest, 2015
7. F. Wu, A. Saha, S. Chaudhuri, C.K. Law, Proc Combust Inst, 35 (2015), 1501

8. C. Ji, E. Dames, Y.L. Wang, H. Wang, F.N. Egolfopoulos, Combust Flame, 157 (2010), 277
9. A.P. Kelley, A.J. Smallbone, D.L. Zhu, C.K. Law, Proc Combust Inst, 33 (2011), 963
10. Paper Part 1
11. Bradley, D., Harper, C.M., Combust Flame 99 (1994) 562
12. Law, C.K., Symp (Inter) Comb 22 (1989) 1381
13. Bechtold, J.K., Matalon, M., Combust Flame 127 (2001) 1906
14. Bradley, D., Sheppard, C.G.W., Woolley, R., Greenhalgh, D.A., Lockett, R.D., Combust Flame 122 (2000) 195
15. Mandilas, C., PhD Thesis, University of Leeds, "Laminar and Turbulent Burning Characteristics of Hydrocarbon Fuels, 2008
16. Wu F., Jomaas G., Law C.K., Fall Technical Meeting of the Eastern States Section of the Combustion Institute Hosted by the University of Connecticut, 2011
17. Zeldovich Y.B., Barenblatt G.I., Librovich V.B., Makhviladze G.M., Mathematical Theory of Combustion and Explosion, Plenum Publ. Corp., N.Y.,1985
18. Kee, R.J., Grcar, J.F., Smooke, M.D., Miller, J.A., A FORTRAN Program for Modeling Steady Laminar One-dimensional Premixed Flames, Sandia Report, SAND85, 8240, Sandia National Laboratories, 1985
19. Grcar, J.F., Kee, R.J., Smooke, M.D., Miller, J.A., Proc Combust Inst 21 (1986) 1773
20. H. Wang, E. Dames, B. Sirjean, D.A. Sheen, R. Tangko, A. Violi, et al., A High temperature Chemical Kinetic Model of n-Alkane (up to n-Dodecane),Cyclohexane, and Methyl-, Ethyl-, n-Propyl and n-Butyl-Cyclohexane Oxidation at High Temperatures, University of Southern California, 2010
21. Egolfopoulos, F.N., Zhu, D.L., Law, C.K., Symp (Inter) Comb 23 (1991) 471
22. Hu, E., Huang, Z., He, J., Miao, H., Int J Hydrogen Energ 34 (2009) 8741
23. Dryer, F.L., Westbrook, C.K., Prog Energ Combust 10 (1984) 1
24. Johnston, R.J., Farrell, J.T., P Combust Inst 30 (2005) 217
25. Gaughan, R., Private Communication, 2007
26. Ormsby, M.P., Turbulent Flame Development in a High-Pressure Combustion Vessel, University of Leeds, 2005, Thesis
27. Zimont, V.L., Exp Therm Fluid Sci 21 (2000) 179
28. Wohl, K., Shore, L., Ind. Eng. Chem. (1955) 828

29. Lipatnikov, A.N., Chomiak, J., Prog Energ Combust 31 (2005) 1
30. Bedat, B., Cheng, R.K., Combust Flame 100 (1995) 485
31. Haq, M.Z., Sheppard, C.G.W., Woolley, R., Greenhalgh, D.A. and Lockett, R.D., Combust Flame 131(2002) 1
32. Bell, J.B., Cheng, R.K., Day, M.S., Shepherd, I.G., Proc Comb Inst 31 (2007) 1309
33. Lawes, M., Ormsby, M.P., Sheppard, C.G.W., Woolley, R., Combust Sci Technol 177 (2005) 1273
34. Aspden, A.J., Day, M.S., Bell, J.B., Proc Comb Inst 33 (2011) 1463
35. Day, M.S., Gao, X., Bell, J.B., Proc Comb Inst 33 (2011) 1601
36. Bradley, D., Lau, A.K.C., and Lawes, M., Phil Trans R Soc 338 (1992) 359
37. Borghi, R., Prog Energ Combust 14 (1988) 245
38. Venkateswaran, P., Marshall, A., Seitzman, J., Lieuwen, T., Proc Comb Inst 34 (2013) 1527
39. Lawes, M., Ormsby, M.P., Sheppard, C.G.W., Woolley R., Combust Flame, 159 (2012) 1949
40. Bray, K.N., Peters, N., Turbulent Reactive Flows – Laminar Flamelets in Turbulent Flows, Academic Press, 1994
41. Weiß, M., Zarzalis, N., Suntz, R., Combust Flame 154 (2008) 671S
42. Driscoll, J.F., Prog Energ Combust Sci 34 (2008) 91